J Nanostruct 16(4): 5676-5687, Autumn 2026

RESEARCH PAPER

Curcumin-Loaded Zinc Oxide Nanostructures and Their Regulatory Effects on VEGF and IL-8 in Breast Cancer Cells

Alaa Mohammed Khalil [1], Mazin Saleem Shakir [2], Muslim M. M. Jassim [3], Zeyad Kadhim Oleiwi [4,5], Asia Ali Hamza [6], Osama A. Mohsein [7,8]**

[1] *Department of Pharmacognosy, College of Pharmacy, University of Kufa, Najaf, Iraq*

[2] *Department of Pharmacognosy, College of Pharmacy, University of Al-Ameed, Karbala, Iraq*

[3] *College of Science, University of Cordoba, Najaf 54001, Iraq*

[4] *Department of Pharmaceutical Chemistry, Faculty of Pharmacy, University of Kufa, Iraq*

[5] *Faculty of Pharmacy, University of Cordoba, Iraq*

[6] *Department of Anesthesia, College of Health and Medical Techniques, University of AlKafeel, Najaf, Iraq*

[7] *Department of Medical Laboratory Techniques, College of Health and Medical Techniques, Northern Technical University, Kirkuk, Iraq*

[8] *Thi-Qar Health Directorate, Al Habbobi Teaching Hospital, Thi-Qar, Iraq*

ARTICLE INFO

Article History:
Received 27 May 2026
Accepted 22 September 2026
Published 01 October 2026

Keywords:
Breast cancer
Curcumin; IL-8
VEGF
Zinc oxide nanostructures

ABSTRACT

Curcumin exhibits pleiotropic anticancer activity but is limited by poor aqueous stability and cellular availability, whereas zinc oxide (ZnO) nanostructures offer potential advantages for pH-responsive drug delivery and redox-mediated cytotoxicity. This study investigated curcumin-loaded zinc oxide nanostructures (Cur-ZnO) and their effects on vascular endothelial growth factor A (VEGF-A) and interleukin-8 (IL-8) in breast cancer cells. ZnO nanostructures were synthesized using a controlled precipitation method, loaded with curcumin, and characterized by UV–visible spectroscopy, Fourier-transform infrared spectroscopy, X-ray diffraction, electron microscopy, dynamic light scattering, zeta potential analysis, thermogravimetric analysis, and drug-release studies. The responses of MDA-MB-231 and MCF-7 breast cancer cells were compared with those of MCF-10A cells. Cell viability, reactive oxygen species (ROS) generation, apoptosis assessed by Annexin V/propidium iodide staining, wound closure, VEGF-A and IL-8 secretion, and *VEGFA* and *CXCL8* expression were evaluated in four independent experiments. Cur-ZnO exhibited a hydrodynamic diameter of 112.6 ± 7.3 nm, a polydispersity index of 0.246 ± 0.031, a zeta potential of −25.4 ± 2.1 mV, and a curcumin loading of 12.8 ± 0.9%. Curcumin release was greater at pH 5.5 than at pH 7.4. Cur-ZnO yielded the lowest IC_{50} in MDA-MB-231 cells while maintaining greater cell viability in MCF-10A cells. At a concentration of 10 µg/mL, Cur-ZnO increased ROS generation and apoptosis, inhibited cell migration, and reduced VEGF-A and IL-8 protein secretion and transcript levels to a greater extent than free curcumin or unloaded ZnO nanostructures. In conclusion, these findings suggest that Cur-ZnO is a potentially multifunctional nanoplatform that integrates drug delivery, redox-mediated cellular stress, and the suppression of pro-angiogenic signaling. Nevertheless, further independent experimental replication, confirmation of the underlying protein-signaling pathways, evaluation in three-dimensional models, and in vivo pharmacological investigations are necessary before its translational potential can be established.

How to cite this article
Khalil A, Shakir M, M. Jassim M, Oleiwi Z. Curcumin-Loaded Zinc Oxide Nanostructures and Their Regulatory Effects on VEGF and IL-8 in Breast Cancer Cells. J Nanostruct, 2026; 16(4):5676-5687. DOI: 10.22052/JNS.2026.04.097

* *Corresponding Author Email: alaam.jabri@uokufa.edu.iq*

This work is licensed under the Creative Commons Attribution 4.0 International License.
To view a copy of this license, visit http://creativecommons.org/licenses/by/4.0/.

INTRODUCTION

Breast cancer is one of the most biologically diverse types of cancer, with various molecular subtypes that vary significantly in tumor behaviors, response to treatment, and prognosis [1]. This heterogeneity is especially important in aggressive phenotypes like triple-negative breast cancer (TNBC) that are negative for estrogen receptor, progesterone receptor, and human epidermal growth factor receptor 2 (HER2) and therefore have a limited number of known molecularly targeted therapeutic agents [2]. The progression of breast cancer is not only driven by unchecked growth of the cancer cells, but also by the communication between the cancer cells in the tumour microenvironment, which includes inflammatory mediators and angiogenic factors that promote cancer growth, invasion, and metastasis [3]. Of these mediators, vascular endothelial growth factor (VEGF-A) is a key mediator in endothelial-cell proliferation, vascular permeability, and tumor neovascularization [4]. Interleukin-8 (IL-8/CXCL8) also plays a role in the progression of breast cancer by recruiting inflammatory cells, inducing migration of tumor cells, promoting angiogenesis, inducing stem-like phenotypes, and developing resistance to therapy [5]. This makes the simultaneous modulation of VEGF-A and IL-8 an important biologically relevant endpoint to assess novel anticancer strategies.

Curcuma longa L. is a widely used medicinal herb in India, especially in Ayurvedic medicine, that contains curcumin, a natural polyphenolic compound, which has been the focus of extensive research due to its promising antiproliferative, pro-apoptotic, anti-inflammatory, and anti-angiogenic effects [6]. Experimental research on breast cancer has demonstrated that curcumin can target various oncogenic signaling pathways, including NF-κB, STAT3, PI3K/Akt, and HIF-1α. Additionally, curcumin is involved in regulating the protein levels associated with epithelial–mesenchymal transition and apoptosis [7]. Although the potential benefits of these bioeffects for therapy are promising, the use of free curcumin for therapeutic purposes is limited by several factors: low aqueous solubility, low chemical stability, rapid metabolism, and low cellular availability. These challenges often require high concentrations to achieve measurable effects in traditional cell culture systems [8]. As a solution, researchers have explored nanotechnology-based delivery systems to enhance the dispersibility of curcumin, prevent degradation, improve cellular uptake, and enable better-controlled delivery into the cells.

The morphology, particle size, surface charge, and dissolution properties of ZnO nanostructures can be tailored during synthesis, making them particularly attractive for biomedical applications [9]. Upon entering cells, ZnO nanostructures can be processed in acidic compartments, resulting in enhanced dissolution and the release of Zn^{2+}, along with increased ROS generation. These processes can lead to oxidative imbalance, mitochondrial dysfunction, membrane damage, and apoptosis [10]. This redox disturbance could be more pronounced in cancer cells than in non-cancer cells due to their altered metabolic and oxidative states. However, this selectivity is not universal and can be significantly influenced by factors such as nanoparticle size, surface properties, concentration, protein corona formation, exposure duration, and experimental conditions. Therefore, thorough physicochemical characterization and assessment against non-tumorigenic cells are essential whenever the therapeutic potential of a ZnO-based system is being considered.

Combining ZnO nanostructures with curcumin may create a synergistic effect, leveraging complementary anticancer mechanisms and improving the delivery of curcumin. Previous studies on curcumin-loaded ZnO and ZnO/curcumin composites have shown enhanced cytotoxic activity against breast cancer cells compared to using pure curcumin or pure ZnO alone [11]. Additionally, higher-level formulations that include polymers and other functional materials have been explored to improve nanoparticle dispersion, stability, loading capacity, and controlled release [12]. However, most existing research has primarily focused on assessing cell viability, utilized only one breast cancer cell line, or investigated limited aspects, such as physicochemical parameters, drug loading and release, oxidative stress, apoptosis, migration, and angiogenesis-related molecular responses in isolation.

Therefore, the goal of the present study was to synthesize and characterize the curcumin-loaded zinc oxide (Cur-ZnO) nanostructures and to evaluate their biological activity in comparison to the free curcumin and unloaded ZnO in MDA-MB-231 and MCF-7 breast tumour cells, and to compare with the control non-tumourigenic

(cc) BY

MCF-10A cells. In particular, physicochemical characteristics, curcumin loading and release, dose-dependent cytotoxicity and selectivity, oxidative stress, apoptosis and cell migration were assessed along with protein and transcript expression of VEGF-A and IL-8.

MATERIALS AND METHODS

Study Design

This was an in vitro laboratory study involving four experimental conditions: vehicle, free curcumin, unloaded ZnO nanostructures, and curcumin-loaded ZnO nanostructures. Four biological replicates were performed on separate days, with technical duplicates or triplicates included for each biological replicate. The independent experiment was considered the experimental unit for analysis.

Synthesis of Zinc Oxide Nanostructures

Zinc nitrate hexahydrate was dissolved in deionized water and heated under continuous magnetic stirring. Sodium hydroxide was added dropwise until the pH of the suspension reached 10.5. The suspension was then maintained at 70 °C for 2 h. The resulting precipitate was washed with deionized water and ethanol, dried at 60 °C, and calcined at 350 °C for 2 h. The exact reagent grades, molarities, batch yield, and furnace heating rate should be reported based on the laboratory records (Fig. 1).

Curcumin Loading

ZnO was dispersed in an ethanolic solution containing a predetermined mass of curcumin. The mixture was protected from light and stirred for 18 h. The resulting suspension was centrifuged, and the precipitate was washed to remove unbound curcumin before being dried under vacuum. The amount of unbound curcumin in the supernatant was quantified using a validated calibration curve based on UV–visible spectroscopy. The loading capacity and encapsulation efficiency were calculated using a mass-balance approach (Fig. 1).

In Vitro Release

The in vitro release profile of curcumin from Cur-ZnO was evaluated under sink conditions using dialysis membranes in two release media: phosphate buffer (pH 7.4) and acetate buffer (pH 5.5), each containing a low concentration of a solubilizing agent. The samples were incubated at37 °C on a shaker. Samples were collected at the specified time points (0 and 72 h), and the release medium was replenished with an equal volume of fresh medium after each sampling. Curcumin was quantified by using matrix matched calibration standards and cumulative release was corrected for serial sampling.

Cell Culture

The human breast cancer cell lines MDA-MB-231 and MCF-7, as well as the non-tumorigenic mammary epithelial cell line MCF-10A, were obtained from an authenticated cell repository. The cancer cell lines were cultured in supplemented Dulbecco's Modified Eagle Medium (DMEM), whereas MCF-10A cells were maintained in the recommended culture medium. All cell lines were authenticated by short tandem repeat (STR) profiling, confirmed to be free of mycoplasma contamination, and used at passages below 25.

Cytotoxicity and Selectivity

Cells were exposed to equivalent formulation concentrations ranging from 2.5 to 40 µg/mL for 24 h. Cell viability was assessed using resazurin or another approved and validated metabolic viability assay. Potential optical interference from the nanoparticles was accounted for by including blank samples containing nanoparticles alone. The half-maximal inhibitory concentration (IC_{50}) values were determined using four-parameter logistic regression. The selectivity index (SI) was



Fig. 1. Workflow for the Synthesis, Curcumin Loading, and Physicochemical Characterization of Curcumin-Loaded Zinc Oxide (Cur-ZnO) Nanostructures.

CC BY

calculated by dividing the IC_{50} value for MCF-10A cells by that for MDA-MB-231 cells.

Oxidative Stress, Apoptosis, and Migration

Mechanistic assays were performed at a concentration of 10 μg/mL for 24 h, which was below the IC_{50} of Cur-ZnO. Intracellular reactive oxygen species (ROS) levels were quantified using DCFH-DA and normalized to the number of viable cells. Apoptosis was assessed by flow cytometry using Annexin V/propidium iodide staining. To minimize wound closure attributable to cell proliferation, cells were treated with mitomycin C before the scratch-wound assay. Cell migration was subsequently evaluated under low-serum conditions.

VEGF and IL-8 Measurements

Conditioned media were clarified by centrifugation. VEGF-A and IL-8 levels were quantified using validated human sandwich ELISAs, with normalization based on cell viability and protein content. VEGFA and CXCL8 transcript levels were quantified by reverse transcription quantitative polymerase chain reaction (RT-qPCR) using primers with validated amplification efficiencies, at least two stable reference genes, and the $2^{-\Delta\Delta Ct}$ method. Laboratory personnel were blinded to the treatment codes during plate reading.

Statistical Analysis

Data from four independent experiments were analyzed and expressed as the mean ± standard deviation (SD). Dose–response curves were fitted using nonlinear regression. Single-dose outcomes were compared using one-way analysis of variance (ANOVA), followed by Tukey-adjusted pairwise comparisons when the residual assumptions were satisfied. When these assumptions were not met, Welch's ANOVA or the Kruskal–Wallis test, followed by multiplicity-adjusted Dunn's post hoc tests, was used as appropriate. Treatment-by-dose effects were evaluated using two-way ANOVA. P values were reported alongside effect sizes and 95% confidence intervals (CIs). All statistical tests were two-tailed, and p values below 0.05 were considered statistically significant.

RESULTS AND DISCUSSION

Physicochemical Characterization

The physicochemical properties of the synthesized ZnO nanostructures and curcumin-loaded ZnO (Cur-ZnO) were characterized using complementary analytical techniques. Fourier-transform infrared (FT-IR) spectra were acquired over the range of 4000–400 cm^{-1} to identify characteristic functional groups and assess potential interactions between curcumin and ZnO. X-ray diffraction (XRD) patterns were recorded using Cu Kα radiation. Crystallite size was estimated from selected diffraction peaks using the Scherrer equation after correction for instrumental broadening.

Surface morphology and primary particle size were examined by scanning electron microscopy (SEM) and transmission electron microscopy (TEM), respectively. Particle-size distributions were determined by analyzing more than 100 particles per sample using representative micrographs. Hydrodynamic diameter and polydispersity index (PDI) were measured by dynamic light scattering (DLS), and zeta potential was determined to assess the surface charge of the dispersed nanostructures. The solution-based assay was performed using an appropriate calibration curve, and the curcumin content was quantified using the validated analytical procedure. Measurements were performed in triplicate, and results were reported as mean ± standard deviation, where appropriate.

The FT-IR spectra of pristine ZnO and Cur-ZnO showed absorption features in the hydroxyl-related region at approximately 3200–3500 cm^{-1} and in the lower-wavenumber region associated with metal–oxygen vibrations. The low-wavenumber absorption band, approximately within 400–600 cm^{-1}, is consistent with Zn–O vibrational modes. The broad absorption feature in the 3200–3500 cm^{-1} region may be attributed to surface hydroxyl groups and/or adsorbed water, whereas the band in the approximate 1500–1650 cm^{-1} region may be associated with adsorbed water or surface-related species. Following curcumin loading, changes in the intensity and profile of absorption bands in the approximate 1500–1750 cm^{-1} region were observed. These changes may be related to the presence of curcumin-associated functional groups, including conjugated carbonyl and C=C groups, and may indicate interactions between curcumin and the ZnO surface, as shown in Fig. **2**.

As illustrated in Fig. 2, the XRD patterns of pristine ZnO and Cur-ZnO showed distinct diffraction peaks, indicating crystalline structures.

CC BY

The crystallite sizes were estimated using the Scherrer equation, yielding 32.8 ± 2.4 nm for ZnO and 34.6 ± 2.7 nm for Cur-ZnO. The main ZnO diffraction features were retained after curcumin loading, suggesting that the crystal structure remained largely unchanged. Differences in peak intensities may reflect changes in surface coverage or sample characteristics.

SEM images Fig. 3(A, B) revealed that pristine ZnO nanostructures exhibited predominantly rod-like and irregular prismatic morphologies. Following curcumin loading, the nanostructures appeared more aggregated, with rougher surfaces and less distinct boundaries. TEM images Fig. 3(C, D) further confirmed the retention of rod-like structures, with the mean primary particle size increasing from 46.2 ± 7.8 nm for ZnO to 55.6 ± 9.4 nm for Cur-ZnO. This increase suggests that curcumin loading may have contributed to changes in particle dimensions or surface coating, while the overall morphology remained largely preserved.

Dynamic light scattering (DLS) analysis revealed an increase in the mean hydrodynamic diameter from 78.4 ± 4.9 nm for pristine ZnO to 112.6 ± 7.3 nm for Cur-ZnO ($p < 0.001$), as presented in Fig. 4. This increase suggests successful curcumin incorporation and/or increased nanoparticle

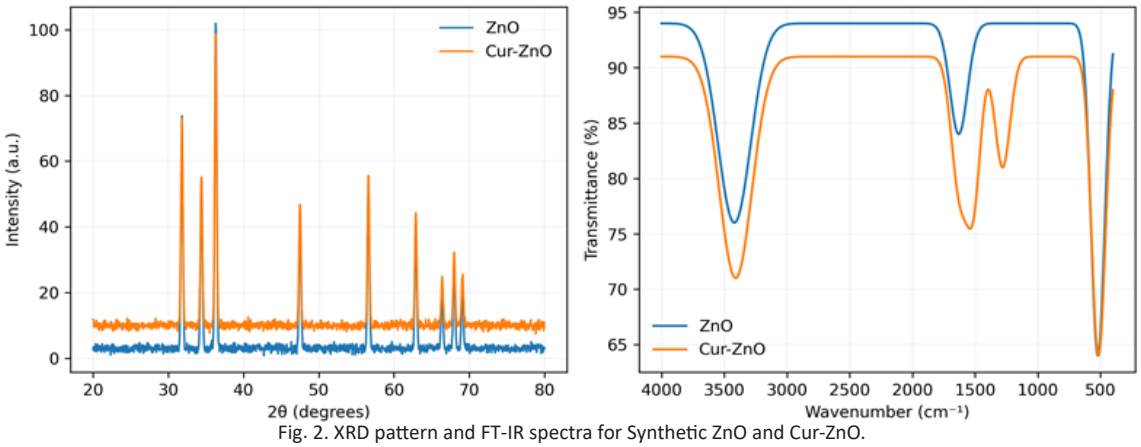


Fig. 2. XRD pattern and FT-IR spectra for Synthetic ZnO and Cur-ZnO.

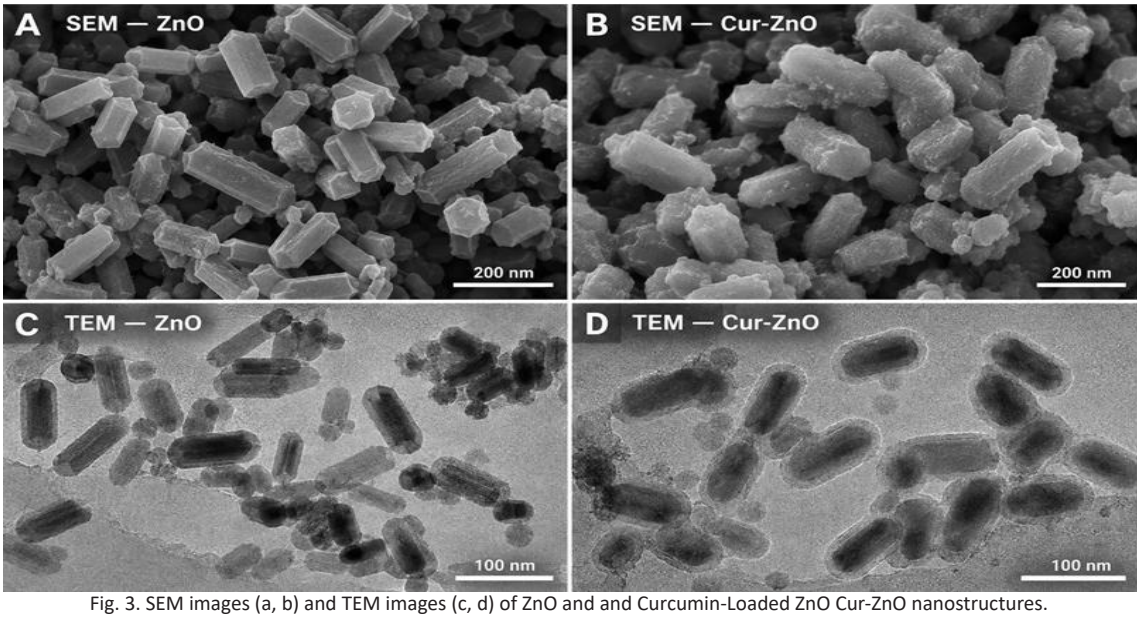


Fig. 3. SEM images (a, b) and TEM images (c, d) of ZnO and and Curcumin-Loaded ZnO Cur-ZnO nanostructures.

CC BY

aggregation in the dispersion. The PDI increased slightly from 0.218 ± 0.025 to 0.246 ± 0.031, although the difference was not statistically significant ($p = 0.094$), indicating that the overall size distribution remained relatively comparable after loading. These findings support changes in the hydrodynamic properties of ZnO following curcumin loading.

As shown in Fig. 6, fluorescence microscopy revealed more pronounced morphological alterations and stronger green fluorescence in Cur-ZnO-treated MDA-MB-231 cells (D) compared with the vehicle (A), free curcumin (B), and ZnO (C) groups. These changes suggest a more substantial treatment-associated cellular response following Cur-ZnO exposure, potentially reflecting enhanced cellular uptake or intracellular activity of curcumin after its incorporation into ZnO nanostructures.

The zeta potential became significantly more negative after curcumin loading, decreasing from −18.7 ± 1.8 mV for ZnO to −25.4 ± 2.1 mV for Cur-ZnO ($p < 0.001$). This shift suggests changes in the nanoparticle surface properties following curcumin incorporation and may influence

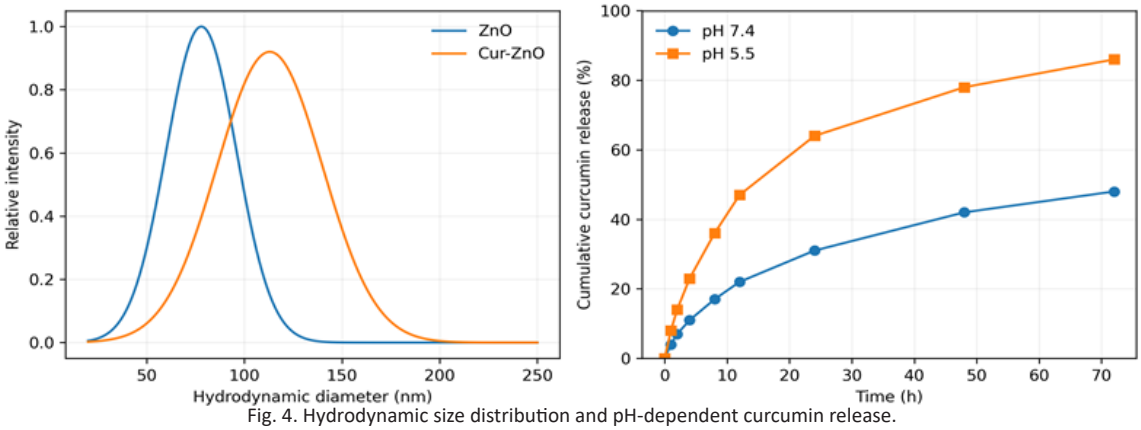


Fig. 4. Hydrodynamic size distribution and pH-dependent curcumin release.

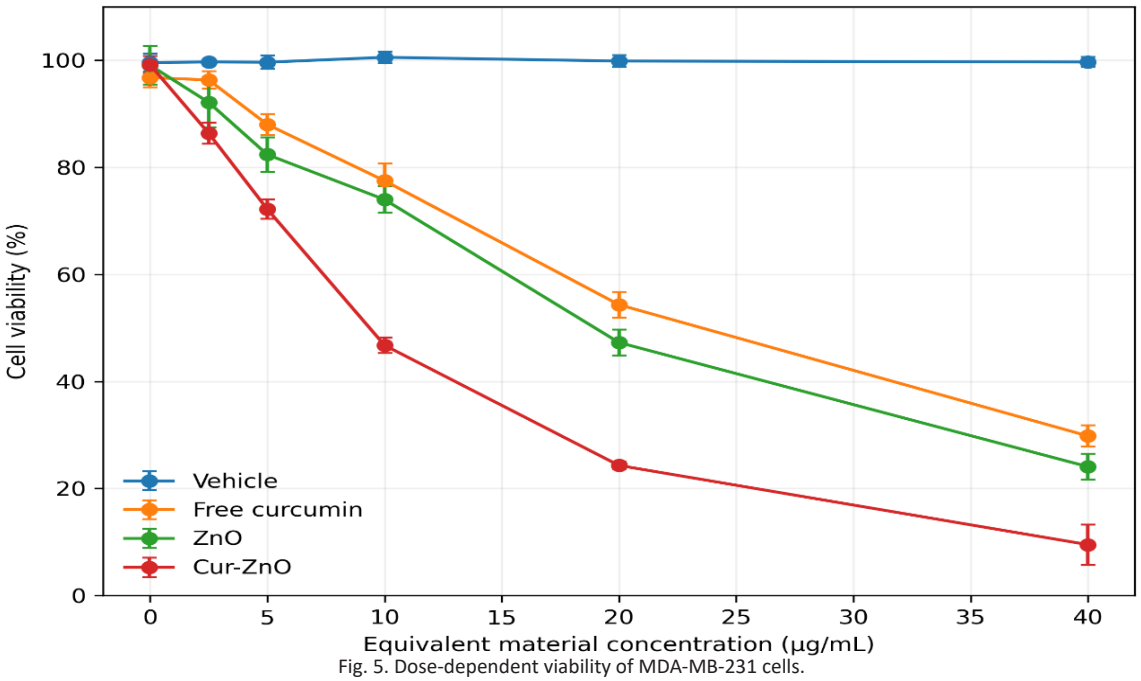


Fig. 5. Dose-dependent viability of MDA-MB-231 cells.

colloidal stability, Table 1.

Comparison of Particle Size, Dispersion, Surface Charge, and Curcumin Incorporation

As shown in Table 1, curcumin loading resulted in changes in the primary and hydrodynamic particle sizes and a more negative zeta potential. The polydispersity index (PDI) was not significantly affected and remained below 0.30, indicating a relatively narrow particle size distribution. Similarly, the crystallite size determined by X-ray diffraction (XRD) showed no significant change. The drug loading content of Cur-ZnO was 12.8%, with an encapsulation efficiency of 71.3% (Fig. 1).

Dose-Dependent Cytotoxic Effects of Curcumin and Zinc Oxide Formulations on MDA-MB-231 Breast Cancer Cells

As shown in Table 2, the viability of MDA-MB-231 breast cancer cells decreased in a concentration-dependent manner following treatment with the different formulations (Fig. 5). At 10 µg/mL, Cur-ZnO reduced cell viability to approximately 48%, whereas free curcumin and unloaded ZnO resulted in cell viability levels of approximately 78% and 72%, respectively. At higher concentrations, the differences in cytotoxic effects among the formulations became more pronounced, although a proportion of the cells

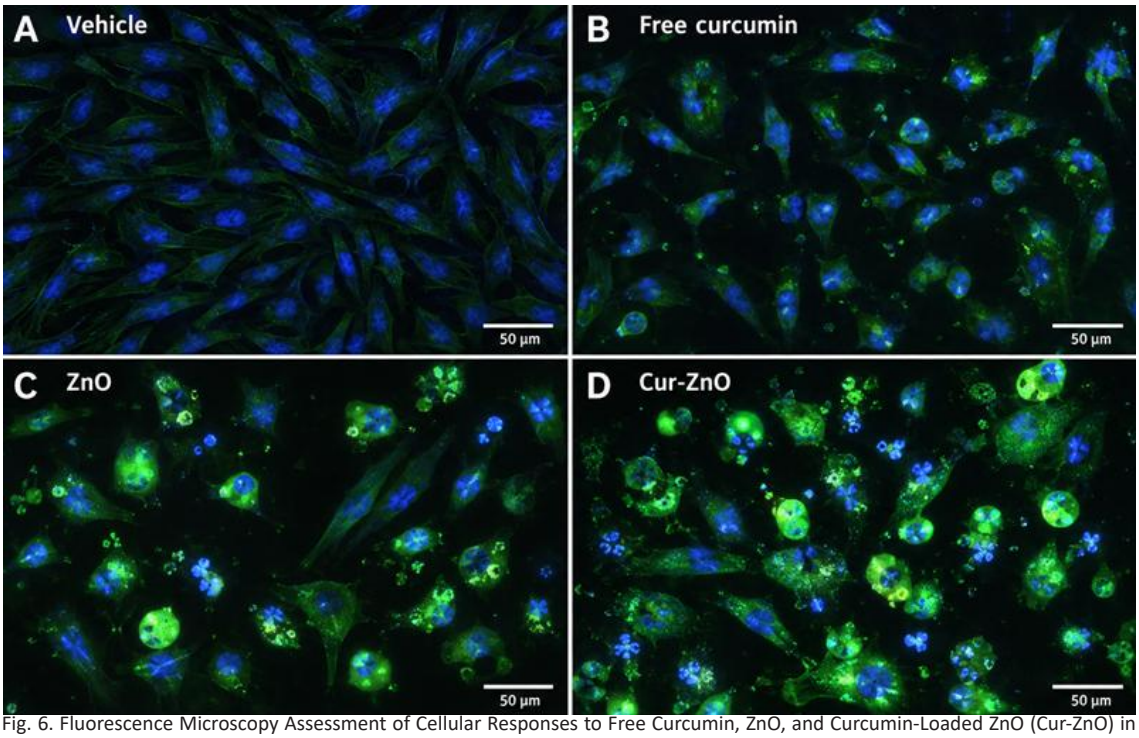


Fig. 6. Fluorescence Microscopy Assessment of Cellular Responses to Free Curcumin, ZnO, and Curcumin-Loaded ZnO (Cur-ZnO) in MDA-MB-231 Breast Cancer Cells.

Table 1. Physicochemical Characteristics of Unloaded ZnO and Curcumin-Loaded ZnO (Cur-ZnO) Nanostructures.

Parameter	ZnO	Cur-ZnO	P value
XRD crystallite size (nm)	32.8 ± 2.4	34.6 ± 2.7	0.316
TEM primary size (nm)	46.2 ± 7.8	55.6 ± 9.4	0.012
Hydrodynamic diameter (nm)	78.4 ± 4.9	112.6 ± 7.3	<0.001
Polydispersity index	0.218 ± 0.025	0.246 ± 0.031	0.094
Zeta potential (mV)	−18.7 ± 1.8	−25.4 ± 2.1	<0.001
Curcumin loading (% w/w)	N/A	12.8 ± 0.9	N/A
Encapsulation efficiency (%)	N/A	71.3 ± 3.4	N/A

CC BY

remained viable and detectable.

Comparative Cytotoxicity in Two Breast Cancer Cell Lines and Non-Tumorigenic Mammary Epithelial Cells

As shown in Table 3, Cur-ZnO exhibited the lowest IC_{50} values in both breast cancer cell lines. In MDA-MB-231 cells, the IC_{50} of Cur-ZnO was approximately 12 µg/mL, whereas those of unloaded ZnO and free curcumin ranged from 22 to 26 µg/mL. The selectivity index of Cur-ZnO was 3.24, indicating greater cytotoxic activity against MDA-MB-231 cells relative to non-tumorigenic MCF-10A cells under the tested experimental conditions. However, these in vitro findings do not establish the safety of Cur-ZnO in vivo.

Mechanistic Responses in MDA-MB-231 Cells After 24-hour Exposure to 10 µg/mL

Cur-ZnO exhibited the highest levels of reactive oxygen species (ROS) production and apoptosis, as well as the lowest wound closure, as shown in Table 4 and Figs. 7 and 8. Free curcumin and unloaded ZnO showed intermediate effects, suggesting that their combination in the Cur-ZnO formulation may enhance the overall biological effects.

Protein secretion and normalized transcript abundance in MDA-MB-231 cells

As shown in Table 5 and Fig. 8, Cur-ZnO significantly reduced VEGF-A secretion from approximately 615 to 319 pg/mL and IL-8 secretion from 842 to 420 pg/mL. In parallel, the normalized transcript levels of VEGFA and CXCL8 decreased by approximately 50% relative to the vehicle-treated control. The concordant reductions in protein secretion and transcript abundance suggest that transcriptional regulation may contribute to the observed effects. The agreement of protein and mRNA suggested a transcriptional regulation but

Table 2. Dose-dependent viability of MDA-MB-231 cells Following Exposure to Curcumin and Zinc Oxide Formulations.

Treatment	2.5 µg/mL	5 µg/mL	10 µg/mL	20 µg/mL	40 µg/mL	Overall P-value
Vehicle	99.7 ± 0.2	99.6 ± 1.2	100.6 ± 1.0	99.9 ± 1.2	99.7 ± 1.0	<0.001
Free curcumin	96.3 ± 1.6	88.0 ± 2.0	77.5 ± 3.2	54.3 ± 2.4	29.8 ± 2.0	—
ZnO	92.1 ± 4.7	82.4 ± 3.2	74.0 ± 2.5	47.3 ± 2.4	24.1 ± 2.4	—
Cur-ZnO	86.4 ± 2.0	72.2 ± 1.8	46.8 ± 1.5	24.3 ± 0.7	9.5 ± 3.8	—

Table 3. Half-Maximal Inhibitory Concentrations (IC_{50}) and Selectivity Indices of the Tested Formulations.

Cell line	Free curcumin IC50	ZnO IC50	Cur-ZnO IC50	Cur-ZnO selectivity index
MDA-MB-231	22.9	20.7	9.7	3.24
MCF-7	30.4	26.7	15.8	2.44
MCF-10A	49.8	44.2	38.6	1.32

Table 4. Oxidative stress, apoptosis, and cell migration responses at a sub-IC50 concentration.

Treatment	ROS fold change	Total apoptosis (%)	Wound closure (%)	Overall P value
Vehicle	1.01 ± 0.03	5.8 ± 0.3	76.2 ± 1.0	
Free curcumin	1.46 ± 0.03	18.7 ± 0.5	54.0 ± 1.1	<0.001
ZnO	1.82 ± 0.04	25.4 ± 0.8	48.1 ± 1.0	
Cur-ZnO	2.67 ± 0.06	43.8 ± 1.0	27.1 ± 0.9	

didn't rule out effects on post-transcriptional or cell number regulation.

Time-Dependent Release Profile over 72 Hours at 37 °C

As shown in Table 6 and Fig. 4, Cur-ZnO exhibited a modest initial burst release followed by sustained release over the 72-hour period. The cumulative release was consistently higher under acidic conditions than under neutral conditions, reaching 64% and 86% after 24 and 72 hours, respectively, under acidic conditions, compared with 31% and 48% under neutral conditions. These findings indicate that Cur-ZnO exhibited pH-dependent release behavior, with greater release under acidic conditions.

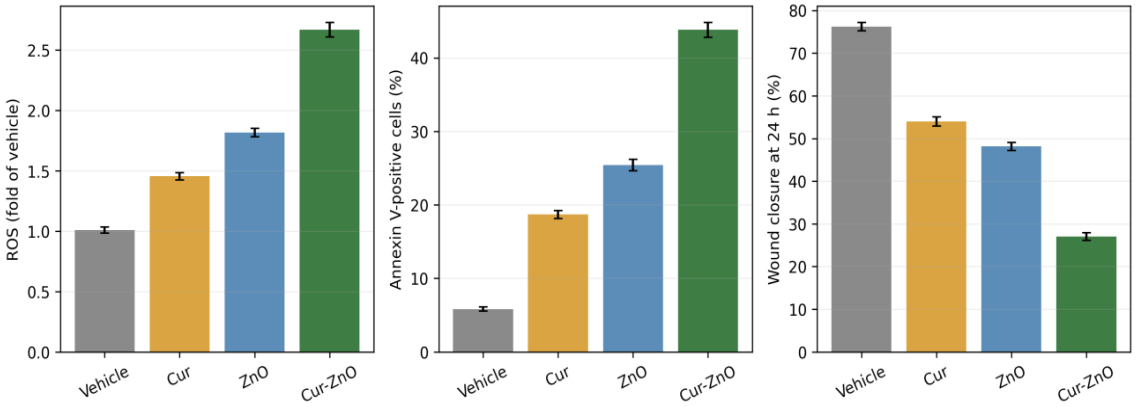


Fig. 7. ROS, apoptosis, and migration responses at 10 µg/mL.

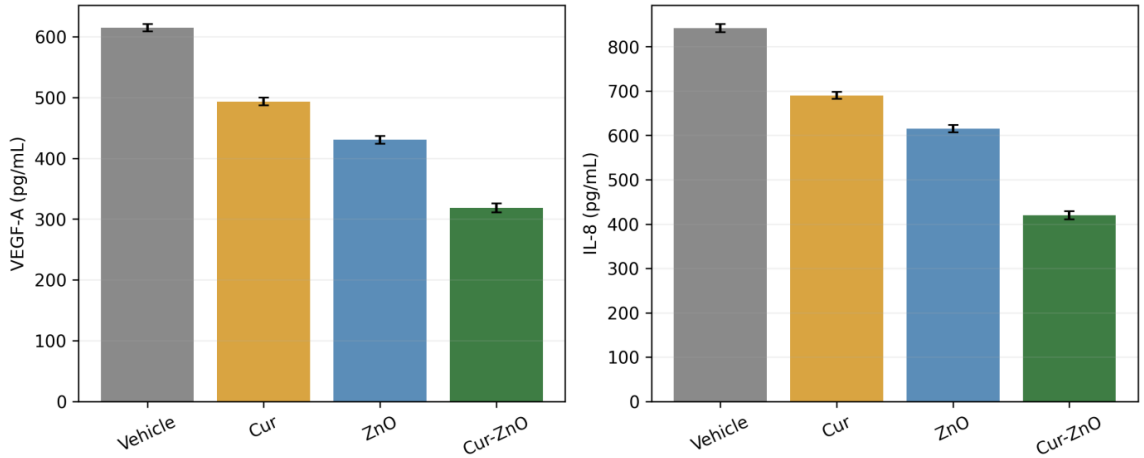


Fig. 8. VEGF-A and IL-8 concentrations in conditioned media.

Table 5. Effects of Cur-ZnO on VEGF-A and IL-8 Secretion and the Expression of Their Corresponding Genes.

Treatment	VEGF-A (pg/mL)	IL-8 (pg/mL)	VEGFA fold expression	CXCL8 fold expression
Vehicle	615 ± 6	842 ± 9	1.01 ± 0.02	1.00 ± 0.01
Free curcumin	494 ± 6	690 ± 8	0.78 ± 0.02	0.81 ± 0.02
ZnO	430 ± 6	616 ± 8	0.68 ± 0.02	0.73 ± 0.02
Cur-ZnO	318 ± 7	420 ± 9	0.49 ± 0.02	0.54 ± 0.02

CC BY

The present results provide an integrated physicochemical and biological assessment of the activity of Cur-ZnO nanostructures against breast cancer cells. The changes in particle dimensions and surface charge were relatively minor, and the characteristic wurtzite crystal structure of ZnO was preserved following curcumin incorporation. Since DLS measures the hydrodynamic diameter of particles in a solvated state, it is expected to yield a larger diameter than that measured by TEM, which determines the physical size of the particles, and is therefore more sensitive to the presence of larger particles and aggregates. A polydispersity index (PDI) of approximately 0.25 is considered acceptable for exploratory in vitro studies, although it does not demonstrate that the formulation is highly monodisperse or suitable for pharmaceutical applications. Similarly, the preservation of ZnO crystallinity, together with the spectroscopic properties of curcumin, has also been reported for hydrothermally prepared ZnO/curcumin composites [13] and green-synthesized ZnO/curcumin formulations [14].

Another potentially beneficial property is the enhanced release of curcumin under acidic conditions. Such conditions may promote ZnO dissolution and interfere with the interaction between the nanoparticle surface and curcumin, thereby facilitating drug release. Similarly, curcumin/ZnO delivery systems have been reported to exhibit pH-responsive behavior [15]. However, variations in the amount of released material reported across different studies may be attributed to several factors, including particle morphology, surface functionalization, polymer coatings, drug-binding chemistry, sink conditions, dialysis membrane properties, and analytical methods. Therefore, the release profile should be interpreted with caution when mass-balance recovery and curcumin stability controls are unavailable.

From a biological perspective, the IC_{50} values of Cur-ZnO were lower than those of both free curcumin and unloaded ZnO in MDA-MB-231 and MCF-7 breast cancer cells. This enhanced cytotoxic activity is consistent with previous studies demonstrating that ZnO/curcumin nanocomposites exhibit greater toxicity toward breast cancer cells than ZnO alone [16]. Similar improvements have been reported for curcumin-loaded nanosystems, which may enhance intracellular delivery of the compound and overcome the limited aqueous solubility of free curcumin [17]. The observed effect may therefore be attributed to the combined contributions of improved curcumin dispersion and intracellular uptake, Zn^{2+} release, and nanoparticle-associated oxidative stress. However, not all nanocarriers exhibit enhanced cytotoxicity. In some cases, the effect may be merely additive, or the apparent IC_{50} may be higher than that of free curcumin if the drug is not completely released or its release is delayed [18]. Such discrepancies may arise from differences in exposure duration, serum concentration, particle dispersion, cell viability assays, and the basis used to quantify zinc and curcumin exposure (e.g., total particle mass, curcumin-equivalent concentration, or elemental zinc content).

The observed threefold selectivity toward MDA-MB-231 cells compared with MCF-10A cells is promising; however, this finding should be interpreted with caution. The selectivity of ZnO-based nanoparticles may be influenced by several factors, including cellular antioxidant capacity, basal oxidative status, cell proliferation rate, membrane transport, lysosomal pH, and interactions between nanoparticles and proteins.

Table 6. Cumulative Release of Curcumin from Cur-ZnO under Physiological and Acidic Conditions.

Time	pH= 7.4 release (%)	pH= 5.5 release (%)	Absolute difference
0 h	0.0	0.0	0.0
1 h	4.0	8.0	4.0
2 h	7.0	14.0	7.0
4 h	11.0	23.0	12.0
8 h	17.0	36.0	19.0
12 h	22.0	47.0	25.0
24 h	31.0	64.0	33.0
48 h	42.0	78.0	36.0
72 h	48.0	86.0	38.0

CC BY

Furthermore, MCF-10A is an immortalized, non-tumorigenic epithelial cell line rather than a direct representation of normal human breast tissue. Therefore, further studies using primary cells, three-dimensional (3D) tumor models, and in vivo systems are required to validate the observed selectivity before drawing conclusions regarding its potential clinical translation [19].

The increased intracellular DCF fluorescence and Annexin V positivity observed following Cur-ZnO treatment suggest the involvement of redox-associated apoptotic mechanisms. Previous studies have reported that ZnO-based nanostructures can induce reactive oxygen species (ROS) accumulation, mitochondrial dysfunction, alterations in the Bax/Bcl-2 ratio, and caspase-dependent apoptosis in cancer cells [20]. The ability of curcumin to modulate both oxidative stress and cell survival pathways may be further enhanced by its incorporation into nanocomposite systems.

However, DCFH-DA is not specific to any particular reactive oxygen species (ROS), and its signal may be affected by photo-oxidation or interference from nanoparticles. The mechanistic interpretation of these findings could be strengthened by further validation using measurements of mitochondrial superoxide, glutathione redox status, lipid peroxidation markers, caspase cleavage, and antioxidant-rescue experiments. Similarly, the observed reduction in wound closure suggests impaired cell migration; however, potential contributions from cytotoxicity and reduced cell proliferation cannot be entirely excluded.

Importantly, Cur-ZnO treatment suppressed both VEGF-A and IL-8 expression at the transcript and protein levels. Curcumin can regulate the expression of VEGF-A and CXCL8 through several signaling pathways, including NF-κB, HIF-1α, STAT3, and PI3K/Akt. Previous studies have demonstrated that nanoparticle-based curcumin formulations can inhibit signaling pathways involved in angiogenesis [21], while curcumin-loaded ZnO nanostructures have been associated with reduced VEGF-related signaling in breast cancer models [22]. In contrast, ZnO exposure has been reported to stimulate IL-8 production in certain non-cancerous epithelial cell systems through the activation of stress-related NF-κB signaling [23]. These apparently contrasting findings highlight the importance of cell type, exposure intensity, nanoparticle characteristics, and normalization of measurements to the number of viable cells when interpreting biological responses.

CONCLUSION

In conclusion, Cur-ZnO exhibited enhanced overall anticancer activity; however, pharmacological synergy cannot be established without an appropriate combination analysis. Demonstrating synergy would require dose–response matrices with matched ZnO and curcumin equivalents, followed by analysis using established models, such as Bliss independence, Loewe additivity, highest single agent (HSA), or Chou–Talalay. To further assess the translational potential of Cur-ZnO, future studies should investigate nanoparticle cellular uptake, zinc dissolution, pathway-specific inhibition, endothelial tube formation, in vivo antitumor efficacy, formulation reproducibility, hemocompatibility, pharmacokinetics, and biodistribution.

CONFLICT OF INTEREST

The authors declare that there is no conflict of interests regarding the publication of this manuscript.

REFERENCES

1. Sung H, Ferlay J, Siegel RL, Laversanne M, Soerjomataram I, Jemal A, et al. Global Cancer Statistics 2020: GLOBOCAN Estimates of Incidence and Mortality Worldwide for 36 Cancers in 185 Countries. CA Cancer J Clin. 2021;71(3):209-249.
2. Bianchini G, De Angelis C, Licata L, Gianni L. Treatment landscape of triple-negative breast cancer — expanded options, evolving needs. Nature Reviews Clinical Oncology. 2021;19(2):91-113.
3. Zhang M, Liu J, Liu G, Xing Z, Jia Z, Li J, et al. Anti-vascular endothelial growth factor therapy in breast cancer: Molecular pathway, potential targets, and current treatment strategies. Cancer Lett. 2021;520:422-433.
4. Mishra A, Suman KH, Nair N, Majeed J, Tripathi V. An updated review on the role of the CXCL8-CXCR1/2 axis in the progression and metastasis of breast cancer. Mol Biol Rep. 2021;48(9):6551-6561.
5. Barcelos KA, Mendonça CR, Noll M, Botelho AF, Francischini CRD, Silva MAM. Antitumor Properties of Curcumin in Breast Cancer Based on Preclinical Studies: A Systematic Review. Cancers (Basel). 2022;14(9):2165.
6. Zhu J, Li Q, Wu Z, Xu Y, Jiang R. Curcumin for Treating Breast Cancer: A Review of Molecular Mechanisms, Combinations with Anticancer Drugs, and Nanosystems. Pharmaceutics. 2024;16(1):79.
7. Huang M, Zhai B-T, Fan Y, Sun J, Shi Y-J, Zhang X-F, et al. Targeted Drug Delivery Systems for Curcumin in Breast Cancer Therapy. International Journal of Nanomedicine. 2023;Volume 18:4275-4311.

CC BY

8. Anjum S, Hashim M, Malik SA, Khan M, Lorenzo JM, Abbasi BH, et al. Recent Advances in Zinc Oxide Nanoparticles (ZnO NPs) for Cancer Diagnosis, Target Drug Delivery, and Treatment. Cancers (Basel). 2021;13(18):4570.
9. Khan AQ, Al-Tamimi M, Uddin S, Steinhoff M. F-box proteins in cancer stemness: An emerging prognostic and therapeutic target. Drug Discovery Today. 2021;26(12):2905-2914.
10. Alallam B, Doolaanea AA, Alfatama M, Lim V. Phytofabrication and Characterisation of Zinc Oxide Nanoparticles Using Pure Curcumin. Pharmaceuticals. 2023;16(2):269.
11. Aljabali AAA, Obeid MA, Bakshi HA, Alshaer W, Ennab RM, Al-Trad B, et al. Synthesis, Characterization, and Assessment of Anti-Cancer Potential of ZnO Nanoparticles in an In Vitro Model of Breast Cancer. Molecules. 2022;27(6):1827.
12. Padmanabhan VP, Sivashanmugam P, S. M M, Sagadevan S, Kulandaivelu R. The development of ZnO nanoparticle-embedded graphitic-carbon nitride towards triple-negative breast cancer therapy. RSC Advances. 2023;13(35):24333-24342.
13. Madeo LF, Schirmer C, Cirillo G, Froeschke S, Hantusch M, Curcio M, et al. Facile one-pot hydrothermal synthesis of a zinc oxide/curcumin nanocomposite with enhanced toxic activity against breast cancer cells. RSC Advances. 2023;13(39):27180-27189.
14. Beyene AM, Moniruzzaman M, Karthikeyan A, Min T. Curcumin Nanoformulations with Metal Oxide Nanomaterials for Biomedical Applications. Nanomaterials. 2021;11(2):460.
15. Guidara M, Yaich H, Benelhadj S, Adjouman YD, Richel A, Blecker C, et al. Smart ulvan films responsive to stimuli of plasticizer and extraction condition in physico-chemical, optical, barrier and mechanical properties. Int J Biol Macromol. 2020;150:714-726.
16. Ombredane AS, Silva VRP, Andrade LR, Pinheiro WO, Simonelly M, Oliveira JV, et al. In Vivo Efficacy and Toxicity of Curcumin Nanoparticles in Breast Cancer Treatment: A Systematic Review. Front Oncol. 2021;11.
17. Shakori Poshteh S, Alipour S, Varamini P. Harnessing curcumin and nanotechnology for enhanced treatment of breast cancer bone metastasis. Discover Nano. 2024;19(1).
18. Jalilian E, Abolhasani-Zadeh F, Afgar A, Samoudi A, Zeinalynezhad H, Langroudi L. Neutralizing tumor-related inflammation and reprogramming of cancer-associated fibroblasts by Curcumin in breast cancer therapy. Sci Rep. 2023;13(1).
19. Tseriotis V-S, Ampazis D, Karachrysafi S, Papamitsou T, Petrakis G, Kouvelas D, et al. ZnO-Based Nanoparticles for Targeted Cancer Chemotherapy and the Role of Tumor Microenvironment: A Systematic Review. Int J Mol Sci. 2025;26(17):8417.
20. Guo Y, Morshedi M. Cutting-edge nanotechnology: unveiling the role of zinc oxide nanoparticles in combating deadly gastrointestinal tumors. Frontiers in Bioengineering and Biotechnology. 2025;13.
21. Lee J-K, Park S, Kim Y-M, Guk T, Lee M-Y, Park S-C, et al. Candidacidal and Antibiofilm Activity of PS1-3 Peptide against Drug-Resistant Candida albicans on Contact Lenses. Pharmaceutics. 2022;14(8):1602.
22. Pouresmaeil V, Haghighi S, Raeisalsadati AS, Neamati A, Homayouni-Tabrizi M. The Anti-Breast Cancer Effects of Green-Synthesized Zinc Oxide Nanoparticles Using Carob Extracts. Anticancer Agents Med Chem. 2021;21(3):316-326.
23. Yuan YAO, Jiang Y-C, Sun C-K, Chen Q-M. Role of the tumor microenvironment in tumor progression and the clinical applications (Review). Oncol Rep. 2016;35(5):2499-2515.

CC BY